Results in Physics 42 (2022) 105996

Contents lists available at ScienceDirect

Results in Physics

journal homepage: www.elsevier.com/locate/rinp

Findings of inhomogeneity in barrier height of Schottky junction Al/rGO-SnO_2 having anomaly in theoretical and experimental value of Richardson constant: A Gaussian approach

Pubali Das [a], Baishakhi Pal [a], Mrinmay Das [a,b,c], Sayantan Sil [a,d], Dhananjoy Das [a], Animesh Layek [a], Partha Pratim Ray [a,*]

[a] Department of Physics, Jadavpur University, Jadavpur, Kolkata 700032, West Bengal, India
[b] School of Applied and Interdisciplinary Sciences, Indian Association for the Cultivation of Science, Jadavpur, Kolkata 700032, West Bengal, India
[c] Department of Physics, Sister Nivedita University, New Town, Kolkata700156, West Bengal, India
[d] Department of Physics, University of Engineering and Management, University Area, Action Area III, B/5, Newtown, Kolkata 700160, West Bengal, India

ARTICLE INFO

Keywords:
rGO-SnO_2 nanocomposite
Defects
Schottky diode
Barrier height
Interface
Inhomogeneity
Gaussian distribution

ABSTRACT

In this research, the temperature dependent dynamical behavior of Schottky junction Al/rGO-SnO^2 has been investigated with thermionic emission (TE) theory within the temperature regime 303 K to 423 K at interval 20 K. During analysis of electrical charge transport behavior an anomalous change is observed in the value of ideality factor and barrier height with rising temperature for the junction. Experimentally derived Richardson constant (of the order $10^{-5}A/m^2K^2$) using TE theory is exceptionally substandard to the theoretical (of the order $10^6A/m^2K^2$) values. The beauty of this work is to find out the underline physics for this discrepancy in measurement of Richardson constant (might arose due to inhomogeneity in barrier of metal-semiconductor junction) by assuming the Gaussian distribution of the barrier height with TE theory at the junction. It is obvious that the occurrence of barrier inhomogeneity across the junction leading charge transport phenomena which mostly impacting upon the parameters of Schottky diodes and its nature because of intrinsic formation of ripples and ridges. In this study, it is found that the charge transport mechanism is highly follows the single Gaussian distribution. The material characterization and its Schottky behavior in normal temperature had been published elsewhere.

Introduction

Thin film based Metal-Semiconductor (MS) Schottky Barrier Diode (SBD)s [1] have attracted huge attention for its wide range of applications, especially in the micro-electronic devices such as optoelectronic [2], bipolar integrated circuits [3] and high frequency device applications [4]. Several current transport mechanism such as thermionic emission (TE), barrier tunneling and carrier generation-recombination at space charge region have been studied to explain various MS junction. Moreover, for the unique features like high conductivity, wide optical transparency and great compatibility for thin film fabrication, graphene composite has proven itself as an important candidate for application in Schottky barrier diodes (SBDs) [5]. As various defects in the crystalline structure effect on material's characteristics under the impact of different environments, having high grain boundary density graphene composites can be influenced by the operating environment [6]. The current conduction mechanism of SBDs depends upon numerous parameters like the operating temperature of the device, barrier height inhomogeneities at MS junction, internal series resistance, functional bias voltage, process of diode preparation [7]. Moreover, there has been growing interest towards rGO-SnO_2 nanocomposite in bio sensors [8], Schottky diodes etc. [9]. The reported band gap value of rGO-SnO_2 is nearly 3.1 eV for the rutile structured SnO_2 decorated in rGO layers [10]. The performance and reliability of rGO-SnO_2 based SBD is dominated by ideality factor, Schottky barrier height (SBH), active metal semiconductor interface, density of interface states and internal series resistance at the metal–semiconductor (MS) junction [11]. For an ideal SBD, ideality factor is 1 and the barrier height is measured simply by the difference between the work function of the metal and the electron affinity of the semiconductor [12]. Barrier height (BH) influences

* Corresponding author.
E-mail address: parthap.ray@jadavpuruniversity.in (P.P. Ray).

https://doi.org/10.1016/j.rinp.2022.105996
Received 18 July 2022; Received in revised form 11 September 2022; Accepted 15 September 2022
Available online 16 September 2022

depletion layer width as well as charge transport mechanism through the MS junction. Usually, the electrical characteristics of SBD is highly influenced by the quality of interface. The room temperature conductivity and barrier height are not sufficient to understand the whole underlying mechanism. Many efforts have been made to comprehend the barrier height characteristics of rGO-SnO_2 based SBDs as well as the - conduction process at room temperature. A number of theories are reported there to explain some of experimental facts [13,14]. At higher temperatures, metal contact may worsen due to diffusion into semiconductor and prepares a weakened MS junction. The operation at high temperature of SBDs with nanocomposite is often essential in application field. The increasing temperature can perturb the device parameters as well as the performance [15]. Different types of Gaussian distribution models are used to clarify the effectuality of barrier height with temperature. To the best of our knowledge, however, the performance of the Al/rGO-SnO_2/ITO SBD at different temperatures has not yet been documented.

The performance of Al/rGO-SnO_2/ITO SBD with varying temperature from 303 K to 423 K have been studied and reported accordingly. In this analysis, an anomalous dependency of barrier height and ideality factor on temperature is observed. This anomalous behavior is clarified and demonstrated with a double Gaussian distribution (GD) of the BHs around a mean value for this device structure.

Materials and method

Among many of the synthesis process the hydrothermal growth of rGO-SnO_2 is predicted to grow better quality of material. All the reagents taken for synthesis are of analytical grade and are used without further purification. rGO-SnO_2 composite is prepared by hydrothermal method (at 160℃ for 12hr) where GO is obtained from modified Hummer's method as reported in the previous work [9].

Experimental

Material characterization

To get idea about crystalline phase of the rGO-SnO_2 before and after heat treatment, powder X-ray diffraction test was performed by Bruker D8 X-ray diffractometer, using Cu Kα radiation. UV–vis spectroscopy data was recorded using Lambda 365 UV–Visible spectrometer. A Quantachrome Autosorb-iQ adsorption device is used to perform a N_2 gas adsorption investigation at 77 K with the desolvated form of rGO–SnO_2 maintained by a liquid-nitrogen bath and pressures varying from 0 to 1 bar for BET measurement. Thermogravimetric analysis (TGA) is performed with the help of METTLER TOLEDO TGA/SDTA-851-e. Without any further purification, a highly pure quality of N_2 (99.9999 %) is used to conduct the analysis.

Device fabrication

A Schottky device with a configuration of Al/rGO-SnO_2/ITO was fabricated by thin film technique as reported earlier [9]. The thickness of rGO-SnO_2 film was measured about 1 μm by the surface profiler and area of the diode was maintained as 7.065×10^{-6} m^2 with the help of shadow mask.

Device characterization

For electrical analysis, Current-voltage (I-V) data was recorded using Keithley 2635 B source meter interfaced with computer under dark condition. Temperature was controlled using a PID controller oven.

Result and discussion

Powder XRD analysis

The powder XRD is a common and useful technique to characterize nanoscale material. The change in dislocation density due to the change in crystallite size on thermal treatment of the nanocomposite material can also be determined from XRD data using Scherrer equation [16]. Fig. 1 shows powder XRD patterns of rGO-SnO_2 nanocomposite before and after heat treatment. The pattern obtained after heat treatment is broadened followed by decrease in peak intensity of the material that might have occurred due to the change in crystallites' size and hence effective surface area. Using the Scherrer equation, the crystallite size and dislocation density of rGO-SnO_2 nanocomposite for each hkl plane (fitted with JCPDS 77-0452 of SnO_2) before and after heat treatment are estimated and given in Table 1. Increase in dislocation density for each hkl plane after heat treatment assures defects increment in material [17]. This increment might impact upon the optical absorption of the derived material.

UV–Visible spectroscopy analysis

The optical absorbance spectra are recorded within wavelength range of 230–600 nm. Fig. 2(a & b) represent that the absorption edge is shifted from higher UV region to lower one after heat treatment of the sample. The optical band gap of the rGO-SnO_2 composite at 303 K and 423 K are determined as 2.9 eV and 3.5 eV with the help of Tauc plot [Fig. 2(c & d)] respectively. These optical band gap (E_g) are calculated by extrapolating the linear portion of the plot of $(\alpha h\nu)^2$ vs $h\nu$ [Fig. 2(c & d)] on the energy axis, where ν is the frequency of light and α is the absorption coefficient [18]. Increase in optical bandgap rather a

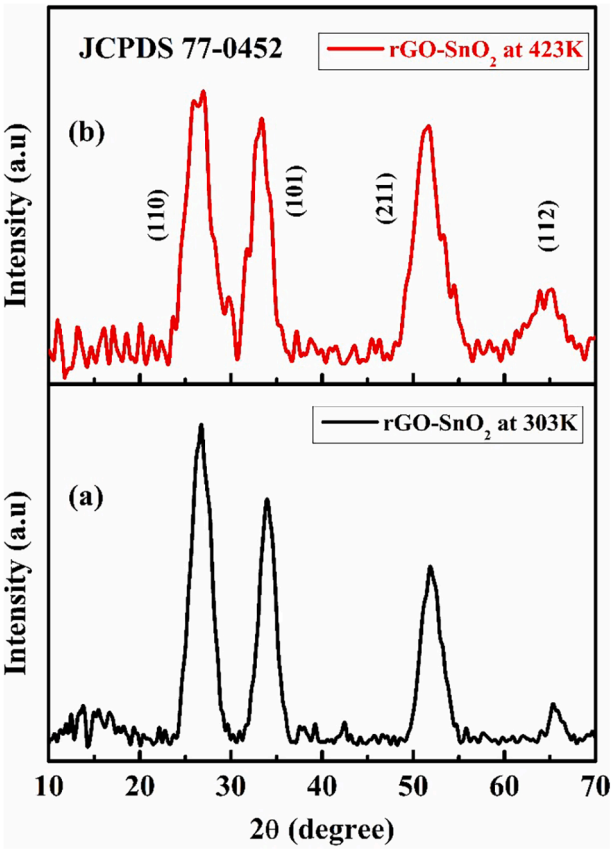

Fig. 1. PXRD patterns of as-prepared rGO-SnO_2 before and after heat treatment.

Table 1
Crystallite size and dislocation density.

Material	Heat Treatment	Plane (*hkl*)	βcosθ	Crystallite size (D) (nm)	Dislocation density (δ) (nm^{-2})
rGO-SnO_2	Before (at303K)	1 1 0	0.0434	3.19	0.098
		1 0 1	0.0348	3.98	0.063
		2 1 1	0.0399	3.47	0.083
		1 1 2	0.0205	6.76	0.022
	After (at423K)	1 1 0	0.0533	2.60	0.148
		1 0 1	0.0411	3.37	0.088
		2 1 1	0.0551	2.51	0.159
		1 1 2	0.0242	5.73	0.030

rigorous change in absorption edge indicates decrease in particle size and hence increase in surface area, which might lead to change in pore size/porosity or occurrence of various interstitial defect states. These interstitial defects impact upon the carrier transport mechanism whenever the sample is introduced within the device.

BET characterization

Electrical conductivity is related to pore-size and porosity of the nanomaterial. The influence on charge conduction mechanism because of defects, arising due to change in specific surface area during formation of interface [19] within device affects the electrical conductivity. To find out pore size, BET is performed for the composite. Fig. 3(a& b) illustrate the hysteresis loops of the nitrogen adsorption/desorption isotherms of the samples collected at 303 K and 423 K respectively through a relative pressure range of 0.1–1. The graphs correspond to the type I isotherm with a type H_2 hysteresis loop. A type H_2 hysteresis loop is frequently linked with ink-bottle pores with random size distributions of cavities and neck. Fig. 3(c & d) represents $1/[V(P_0/P)-1]$ vs P/P_0plots, determined using the BET equation in relative pressure range of $0.05 < P/P_0 < 0.35$. The emergence of a ultra-microporous or nano-porous structure with a high surface area of 205.37 m^2/g (for 303 K) and 357.09 m^2/g (for 423 K) are confirmed by this sort of isotherm, which are accompanied by 0.7713 nm and 0.7049 nm pore size with pore volume 0.144 cc/g and 0.235 cc/g respectively. The results depict that after high (423 K) temperature treatment, the pore size decreases with increasing pore volume and specific surface area accordingly [20]. The increase in specific surface area produces large number of defects at interface [21].

Thermogravimetric analysis

The purpose of this measurement is to determine the purity percentage of rGO in the rGO-SnO_2 composite and to analyze its stability with temperature. The Fig. 4 depicts TGA curves in the temperature range from 30 °C to 800 °C. There are two distinct weight loss pathways for rGO-SnO_2. The dislodgement of absorbed water causes 5 % weight loss in the range of room temperature to 110 °C [22]. The breakdown of oxygen-containing groups causes 4 % mass loss from 110 °C to 425 °C. The weight loss (3.5 %) is attributable to the degradation of the carbon skeleton at high temperatures, between 425 °C and 600 °C. This decomposition process results in considerable weight reduction, showing that the samples are devoid of rGO. So the weight percentage of rGO in composite is 7.5 %. From the analysis, it is concluded that thermal stability of composite is high enough compared to the operating temperature (303 K–423 K) of the device and there is no degradation of composite during the experimental procedure.

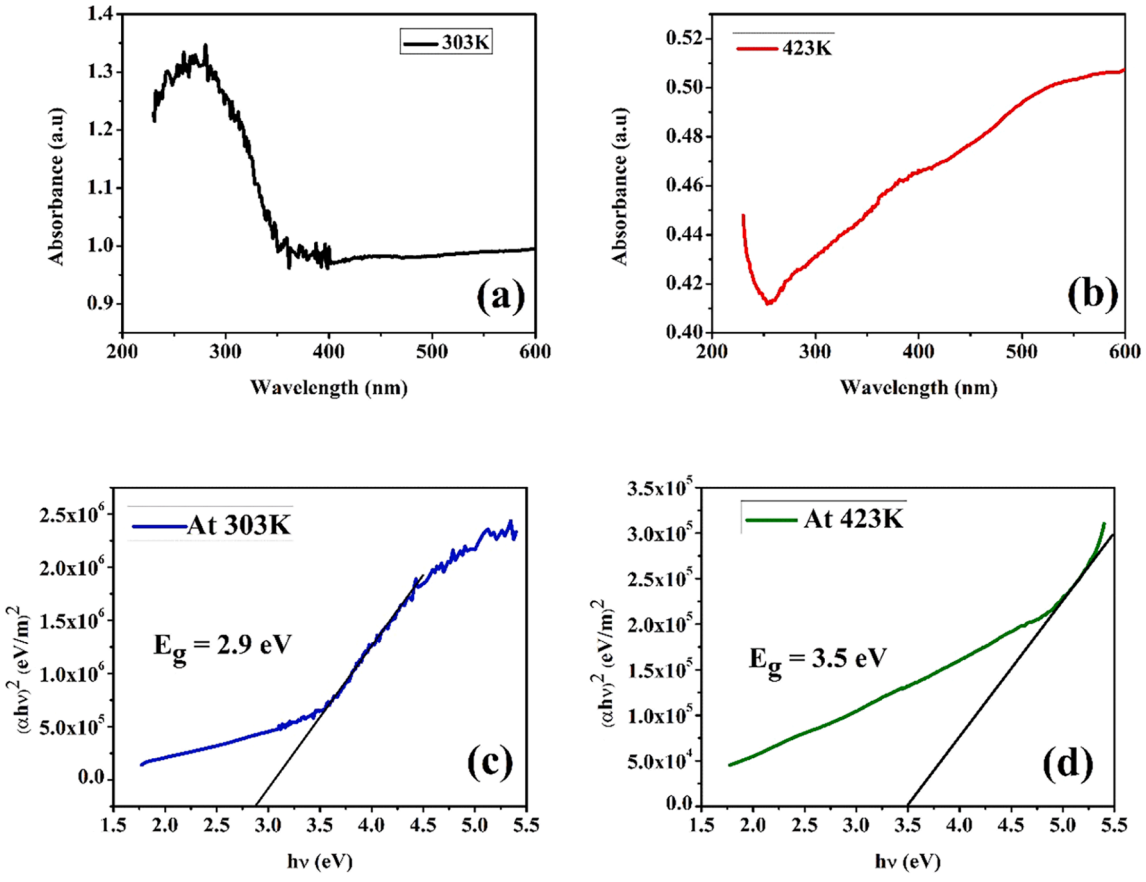

Fig. 2. UV–Visible absorbance spectra and Tauc plot of rGO-SnO_2 at 303 K (a, c) and (b, d) 423 K.

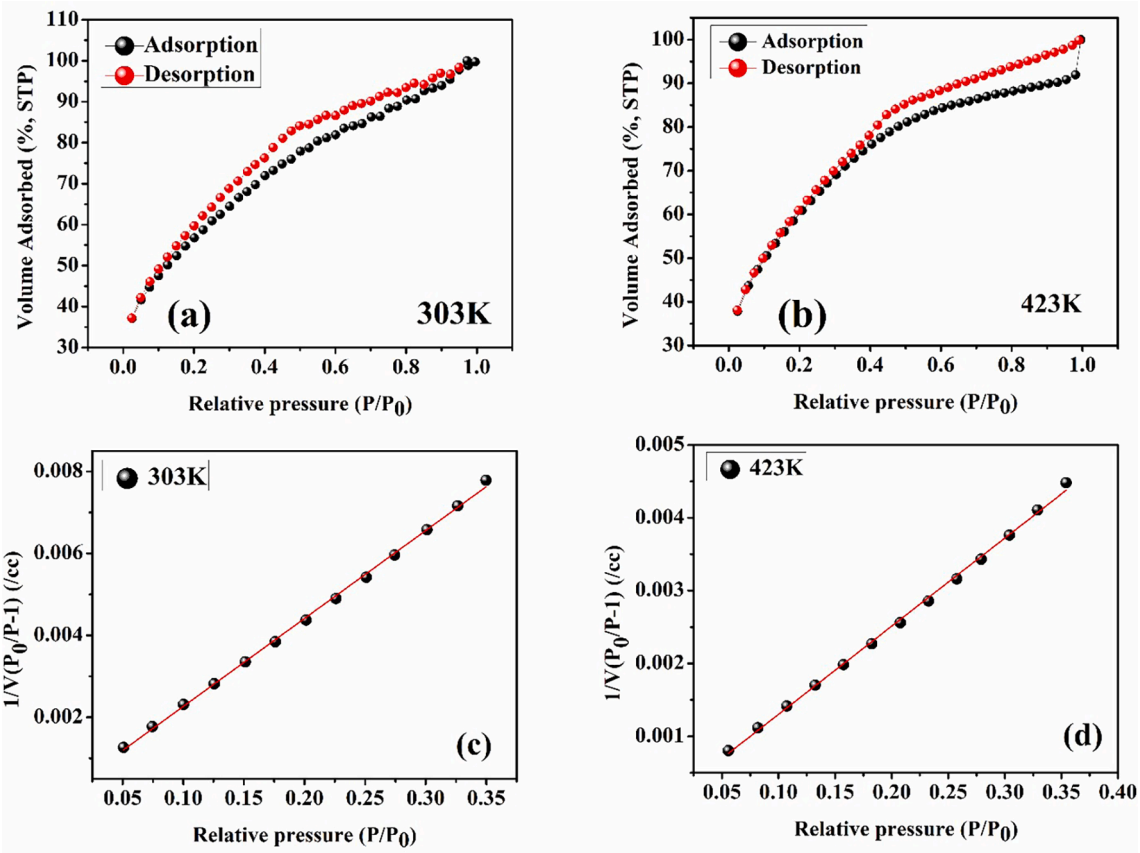

Fig. 3. (a, b) N_2 adsorption–desorption isotherm for rGO-SnO_2 (c, d)1/V(P_0/P-1) variation with relative pressure.

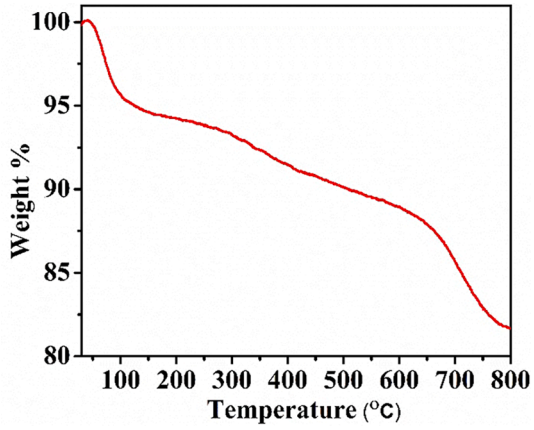

Fig. 4. Thermogravimetric curve for rGO-SnO_2.

Electrical characterization

To intervene into the change in charge transport phenomena of the material at different ambient temperature the current voltage characteristics is recorded for the fabricated device of sandwich structure ITO/rGO-SnO_2/Al. Fig. 5 shows current–voltage (I-V) characteristics of ITO/rGO-SnO_2/Al for the temperature range of 303 K-423 K with an interval of 20 K, which depict rectifying nature implying formation of Schottky barrier diode (SBD). Inset of Fig. 5 exhibits Semi-logarithmic I-V characteristics. Supported by thermionic emission (TE) theory the rectification nature of SBD can be analyzed for a forward bias voltage V (≥3kT/q) by using following equations [23].

$$I = I_0\left[\exp\left(\frac{qV}{\eta kT}\right) - 1\right] \quad (1)$$

And,

$$I_0 = AA^*T^2\exp\left(\frac{-q\varphi_{b0}}{kT}\right) \quad (2)$$

where I_0 is reverse saturation current and q, η, k, T, A, A*,φ_{b0} are the electronic charge, ideality factor, Boltzmann's constant, temperature in Kelvin scale, effective diode area, effective Richardson constant and zero bias barrier height, respectively.

The ideality factor can be measured at each temperature from the slope of forward lnI-V (Fig. 5(b)) plot using the following equation [24,25],

$$\eta = \frac{q}{kT}\left(\frac{dV}{d\ln I}\right) \quad (3)$$

From extrapolation of this plot to V = 0, one can evaluate reverse saturation current. From the value of reverse saturation current, effective BH can be easily estimated by rearranging equation (2) as (eqn. 4) [11],

$$\varphi_{b0} = \frac{kT}{q}\ln\left(\frac{AA^*T^2}{I_0}\right) \quad (4)$$

At higher bias voltage, I-V curve shows deviation from linearity due to interface states and series resistance (R_s). This series resistance is a current limiting factor which differs due to both the bias voltage and applied temperature. The R_s values for different temperature are estimated (Fig. 5(d)) from I to V characteristics curve by using Mikhelashvili method [26], listed in Table 2 (details are in supplementary).

The derived values of ideality factor, reverse saturation current and barrier height are enlisted in Table 2. In this consequence the

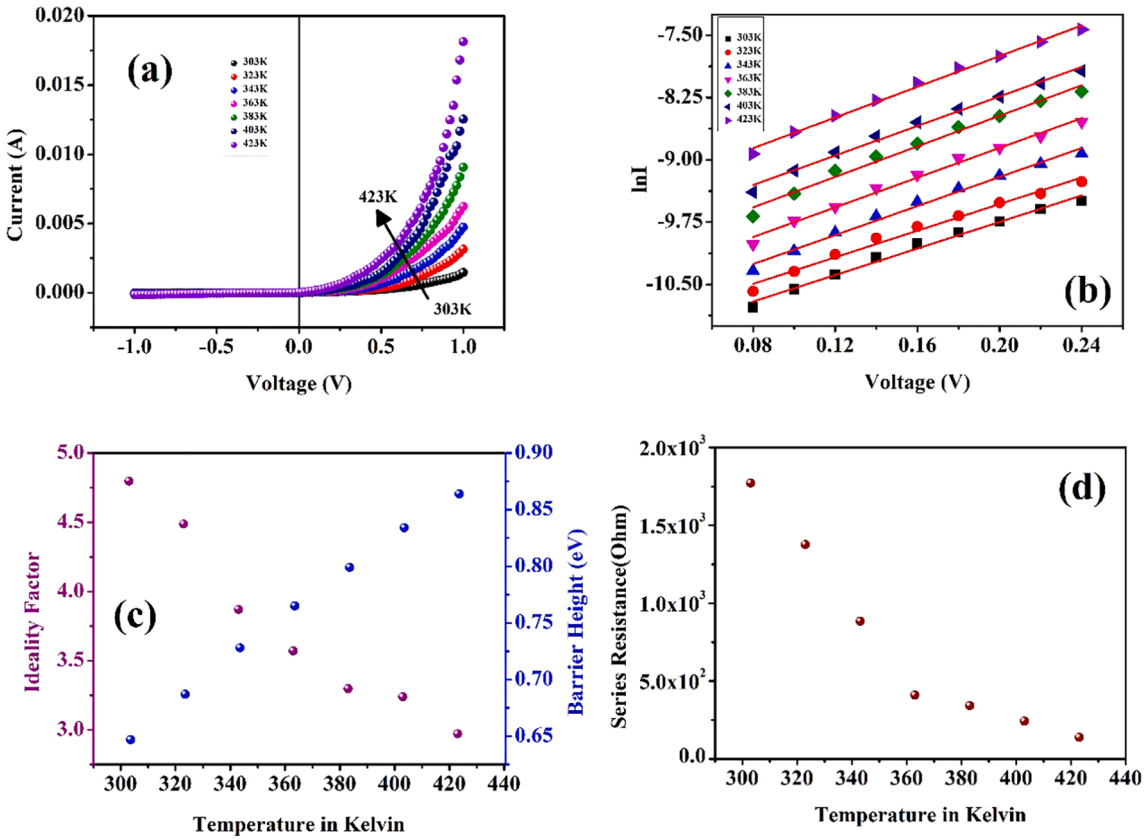

Fig. 5. Temperature variation of (a) I-V characteristics (b) lnI vs V graph (c) ideality factor and barrier height (c) series resistance of Al/rGO-SnO_2/ITO configuration.

Table 2
SBD parameters in different temperature.

T(K)	$I_0 \times 10^{-5}$ (A)	η (IF)	φ_{b0} (eV)	R_s (Ω)
303	1.183	4.797	0.647	1771.48
323	1.461	4.488	0.687	1376.07
343	1.747	3.870	0.728	884.29
363	2.377	3.571	0.765	409.55
383	3.337	3.298	0.799	341.57
403	4.476	3.239	0.834	242.89
423	6.787	2.971	0.864	138.44

Richardson constant is estimated from theoretical approach as illustrated below.

The value of effective mass (m_e*) of rGO-SnO_2 at 303 K and 423 K, are obtained (0.88m_e and 0.9m_e) from the following equation [7],

m_e*=m*m_e.where

$$\frac{1}{m^*} = 1 + \frac{p^2}{2m_e E_g} \quad (1)$$

where m_e(= 9.1 × 10^{-31}kg) is the free electron mass, E_g represents the optical bandgap of rGO-SnO_2 (obtained from optical data) differs with temperature (2.9 eV and 3.5 eV respectively) and momentum p = $\hbar G \approx \hbar/$ a (G is the smallest reciprocal lattice vector and 'a' is the highest lattice constant). The value of 'a' is found to be 0.3199 nm from the JCPDS data which are same for material at temperature 303 K and 423 K. The estimated effective Richardson constant at 303 K and 423 K are 1.057 × 10^6 A/m^2K^2 and 1.081 × 10^6 A/m^2K^2 respectively derived from the equation.

$$A^* = 4\pi m_e^* k^2 q/h^3 \quad (2)$$

where, h is Planck constant.

The change in barrier height and ideality factor with temperature, represented in Fig. 5(c) indicates an increment of barrier height and a decrement of ideality factor with increasing temperature. Fig. 5(d) exhibits decrease in internal series resistance along with temperature. The formation mechanism of barrier height depending upon the thermal treatment could be understood with the help of band diagram (schematic presentation) as indicated below:

Scheme 1 represents certain barrier height, formed in the device at room temperature. With the increase of the temperature, band gap increases i.e. the bands of the semiconductor probably shifted from their previous position creating a high barrier height [27] (given in Table 2).

The high values of ideality factor (Table 2) indicate spatial barrier inhomogeneities and occurrence of interface states at MS junction. The

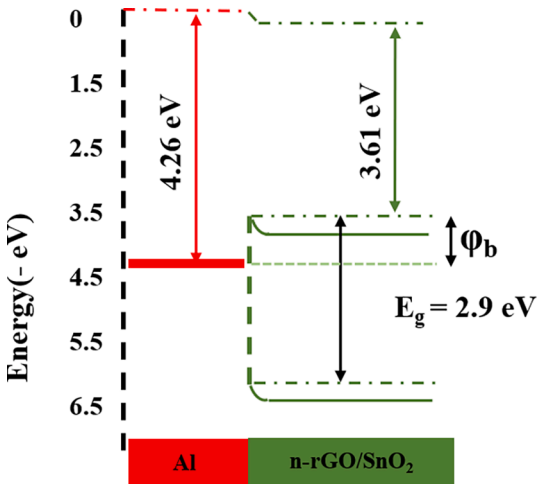

Scheme 1. Schematic Energy band diagram of the MS device.

large value of ideality factor (I.F), highly depends on current transportation mechanism that will be dominated by the electrons impinging through the SBH [28]. In a practical Schottky diode, SBH may not be exactly same over the entire interface area due to a variation in thickness of contact layer, composition of the junction layer and non-uniformity of interfacial charges etc [29]. As conduction of carriers is influenced quite a bit by temperature, at low temperature the conduction electrons can overcome the lower barriers through tunneling [30]. With an increase of temperature, the charge carriers get adequate kinetic energy to overcome the patches of higher barriers through thermionic emission [31,32]. In this study, the barrier height increases with increasing bias voltage and temperature, those attributed to deviation from ideal thermionic emission theory [33].

One should check whether this deviation might influence the value of Richardson constant. For this very purpose, equation (2) is re-written as [34].

$$\ln\left(\frac{I_0}{T^2}\right) = \ln(AA^*) - \frac{q\varphi_{b0}}{kT} \tag{5}$$

The activation energy plot i.e. $\ln(I_0/T^2)$ against q/kT is plotted with the help of equation (5). This plot implies a bowing trend rather than a straight line (while Schottky barrier is independent of temperature). A* can also be evaluated from the intercept (Fig. 6). Fig. 6 shows two linear temperature regions, one from 303 K to 363 K (referred as section I) and other from 383 K to 423 K (referred as section II). These A*s (6.211×10^{-5} A/m^2K^2 for section I and 4.034×10^{-3} $A/m^2K^2$for section II) are much lesser than theoretical values as obtained earlier. The deviation in experimental value of A*is probably due to the existence of charged surface states, metal induced gap states, material defects [35], barrier potential fluctuation of junction [36] etc.

To intervene into the barrier inhomogeneity, φ_{b0} vs η (IF) is plotted and treated by Tung's theoretical approach, a linear relation between φ_{b0} and η (IF) [37]. Fig. 7 interprets the above indicated correlation curve which implies two different linear regions (Reg-I and Reg-II) of different slope. Lateral inhomogeneities of the barrier height may be the cause of occurrence of these two regimes. Considering $\eta = 1$, φ_{b0} are determined as 0.973 eV and 1.199 eV respectively from these plots.

In Fig. 8 for region I the charge transport mechanism is ruled by TE mechanism whereas for region II is ruled by thermionic field emission theory [31]. These two linear regions could be best fitted to two Gaussian distributions (GD) plots, GD I (Reg-I) and GD II (Reg-II) [36]. Here, the GD model is implied to explain the junctional inhomogeneities. This model of inhomogeneous Schottky barrier follows a GD relation [38].

$$P(\varphi_{ap}) = \frac{1}{\sigma_s\sqrt{2\pi}}\exp\left[-\frac{(\varphi_{ap}) - \overline{\varphi}_{b0}}{2\sigma_s^2}\right] \tag{6}$$

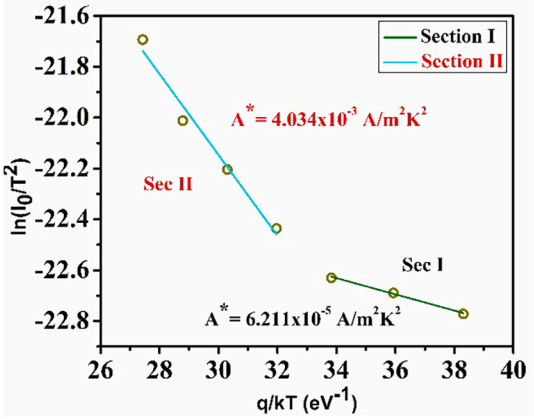

Fig. 6. $\ln(I_0/T^2)$ versus q/kT plot for Al/rGO-SnO_2/ITO configuration.

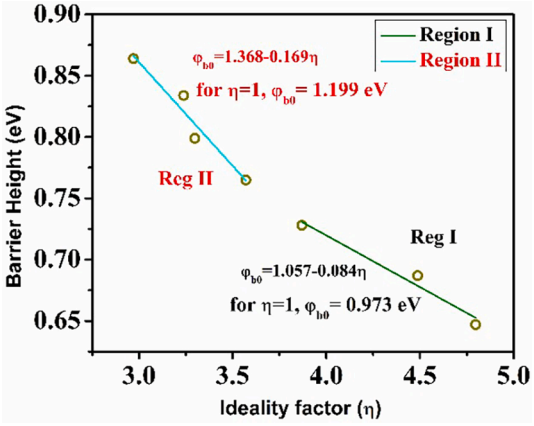

Fig. 7. Barrier height vs Ideality factor for temperature range 303 K to 423 K.

and the related current I(V) is

$$I(V) = \int_{-\infty}^{+\infty} I(\varphi_{ap}, V)P(\varphi_{ap})d\varphi_{ap} \tag{7}$$

where φ_{ap} denotes experimentally measured apparent barrier height and $\frac{1}{\sigma_s\sqrt{2\pi}}$ is the normalization constant of the Gaussian distribution where σ_s is standard deviation.

$I(\varphi_{ap}, V)$ indicates current flow at a bias voltage V according to ideal TE-diffusion (TED) theory and $P(\varphi_{ap})$ is the accuracy probability for BH [39]. In this model φ_{ap} is related to φ_{b0} as,[40].

$$\varphi_{ap} = \varphi_{b0}(T=0) - \frac{q\sigma_s^2}{2kT} \tag{8}$$

To get insight of the best fitted GD (of the type: single or double or multiple) of BH, the plot of φ_{ap} against q/2kT is drawn. Fig. 8a represents two distinct regions within the curve, with two different slopes approving double Gaussian distribution. The slope of each straight line yields the standard deviation whereas intercept gives the barrier potential. Here the value of φ_{b0} is 1.465 eV and 1.339 eV and value of σ_s is 0.19 V and 0.209 V for region I and region II, respectively. Generally lower value of σ_s indicates lower barrier inhomogeneity. As the slopes seemed quite closer in magnitude, there is every possibility to explain the phenomena by using single GD method. By implying single GD method (Eq. (8)), the parameters φ_{b0} and σ_s related with barrier inhomogeneity are estimated as 1.41 eV and 0.2 V (Fig. 8b).

To estimate the modified value of A*with above approach, the Arrhenius equation (eq. (5)) of the form.

$$\ln\left(\frac{I_0}{T^2}\right) - \left(\frac{q^2\sigma_s^2}{2k^2T^2}\right) = \ln(AA^*) - \frac{q\varphi_{b0}}{kT} \tag{9}$$

is considered. Considering the intercept of the extrapolated curve of $\ln(I_0/T^2)$-$q^2\sigma_s^2/2k^2T^2$ against q/kT (Fig. 9) the value of A* is calculated as 1.169×10^6 A/m^2K^2 which is close to the theoretical value.

Conclusion

In this research work the temperature dependent current–voltage relation of Al/rGO-SnO_2/ITO Schottky diode are measured within the temperature range of 303 K-423 K at interval 20 K. While the curves are analyzed to intervene into the charge transport mechanism, an incongruity is observed in the value of ideality factor and barrier height with rising temperature. The value of Richardson constant (of the order $10^{-5}A/m^2K^2$) derived from experimental data by using TE theory is remarkably substandard to the theoretical (of the order $10^6A/m^2K^2$) value. The discrepancy for barrier inhomogeneity is shorted out and illustrated by adopting the Gaussian distribution (of kind single and

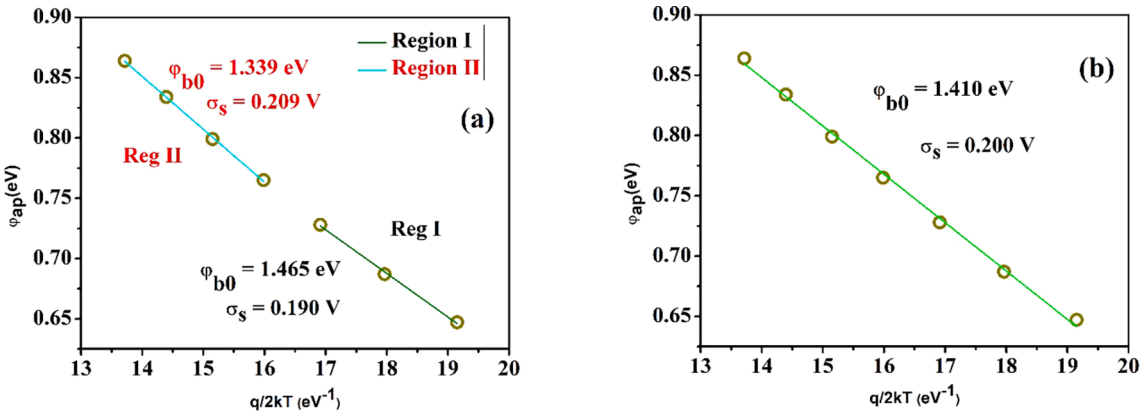

Fig. 8. φ_{ap} against q/2kT plot to check (a) double and (b) single Gaussian.

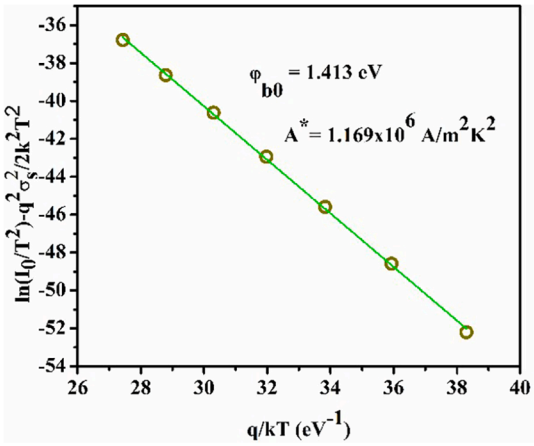

Fig. 9. $\ln(I_0/T^2)$-$q^2\sigma_s^2/2k^2T^2$ against q/kT plot.

double) analysis. The theoretical model of single Gaussian distribution of barrier inhomogeneity approves our approach and is sufficient to provide satisfactory insights of the leading parameters of charge transportation through junction. From the modified Richardson plot, it is confirmed that the evaluated value of Richardson constants are in close agreement to the theoretical values. Thus it can be concluded that the temperature dependent current–voltage (I-V) characteristics of Al/rGO-SnO_2 Schottky junction can be successfully explained based on TE theory assuming a single Gaussian distribution of the barrier height.

Declaration of Competing Interest

The authors declare that they have no known competing financial interests or personal relationships that could have appeared to influence the work reported in this paper.

Data availability

Data will be made available on request.

Acknowledgements

The author would like to thank Department of Science and Technology, Government of India for their fellowship under INSPIRE AORC program. Partha Pratim Ray gratefully acknowledges the financial support of this work by SERB-DST, Govt. of India (Sanction No. EMR/2016/005387 Dated – 24.07.2017).

Appendix A. Supplementary data

Supplementary data to this article can be found online at https://doi.org/10.1016/j.rinp.2022.105996.

References

[1] Guo H, Lang X, Tian X, Jiang W, Wang G. Tunable Schottky barrier in Janus-XGa2Y/graphene (X/Y = S, Se, Te; X ≠ Y) van der Waals heterostructures. Nanotechnology 2022;33(42):425704.
[2] Sannakashappanavar BS, Yadav AB, Byrareddy CR, Narasimha Murty NVL. Fabrication and characterization of Schottky diode on ultrathin ZnO film and its application for UV detection. Mater Res Express 2019;6:116445.
[3] Singh S, Cooper JA. Bipolar integrated circuits in 4H-SiC. IEEE Trans Electron Devices 2011;58(4):1084–90.
[4] Manohara HM, Wong EW, Schlecht E, Hunt BD, Siegel PH. Carbon nanotube Schottky diodes using Ti–Schottky and Pt–ohmic contacts for high frequency applications. Nano Lett 2005;5(7):1469–74.
[5] Das M, Datta J, Dey A, Jana R, Layek A, Middya S, et al. One step hydrothermal synthesis of a rGO–TiO2 nanocomposite and its application on a Schottky diode: improvement in device performance and transport properties. RSC Adv 2015;5(123):101582–92.
[6] Hiltunen V-M, Koskinen P, Mentel KK, Manninen J, Myllyperkiö P, Pettersson M, et al. Ultrastiff graphene. npj 2D Mater Appl 2021;5(1).
[7] Sil S, Jana R, Biswas A, Das D, Dey A, Datta J, et al. Elucidation of inhomogeneous heterojunction performance of Al/Cu5FeS4 Schottky diode with a gaussian distribution of barrier heights. IEEE Trans Electron Devices 2020;67(5):2082–7.
[8] Medha Gijare, Suyog Danane, Manisha Modak, Anil Garje; Synthesis and characterization of rGO + SnO2 composite for bio sensor application, 2019 JETIR May 2019, Volume 6, Issue 5, page no. pp17-22.
[9] Das P, Pal B, Datta J, Das M, Sil S, Ray PP. Improved charge transport properties of graphene incorporated tin oxide based Schottky diode over pure one. J Phys Chem Solids 2021;148:109706.
[10] Van Tuan P, Tuong HB, Tan VT, Thu LH, Khoang ND, Khiem TN. SnO_2/reduced graphene oxide nanocomposites for highly efficient photocatalytic degradation of methylene blue. Opt Mater 2022;123:111916.
[11] Dey A, Jana R, Dhar J, Das P, Ray PP. Gaussian distribution of inhomogeneous barrier height of Al/ZnS/ITO Schottky barrier diodes. Materials Today 2018;5(3):9958–64.
[12] Yüksel ÖF, Tuğluoğlu N, Gülveren B, Şafak H, Kuş M. Electrical properties of Au/perylene-monoimide/p-Si Schottky diode. J Alloy Compd 2013;577(15):30–6.
[13] Schmitsdorf RF, Kampen TU, Mönch W. Explanation of the linear correlation between barrier heights and ideality factors of real metal-semiconductor contacts by laterally nonuniform Schottky barriers. J Vacuum Sci Technol B 1997;15:1221.
[14] Hadj Belgacem C. El-Amine; theoretical models for anomalously high ideality factor in a Au/SnO2-Si(n)/Al solar cell. Silicon 2018;10:1063–6.
[15] Yüksel ÖF, Tuğluoğlu N, Gülveren B, Şafak H, Kuş M. Electrical properties of Au/perylene-monoimide/p-Si Schottky diode. J Alloy Compd 2013;577:30–6.
[16] Monshi A, Foroughi MR, Monshi MR. Modified Scherrer equation to estimate more accurately nano-crystallite size using XRD. WJNSE 2012;02(03):154–60.
[17] Gomathi M, Rajkumar PV, Prakasam A. Study of dislocation density (defects such as Ag vacancies and interstitials) of silver nanoparticles, green-synthesized using Barleria cristata leaf extract and the impact of defects on the antibacterial activity. Results Phys 2018;10:858–64.
[18] Tyagi P, Sharma A, Tomar M, Gupta V. A comparative study of RGO-SnO2 and MWCNT-SnO2 nanocomposites based SO2 gas sensors. Sens Actuators, B 2017;248:980–6.
[19] Hakamada M, Kuromura T, Chen Y, Kusuda H, Mabuchi M. Influence of porosity and pore size on electrical resistivity of porous aluminum produced by spacer method. Mater Trans 2007;48(1):32–6.

[20] Liu D, Zhou W, Wu J, Zhou W, Jiang W. CuO-CeO2/ZSM-5 composites for reactive adsorption of hydrogen sulphide at high temperature. Canad J Chem Eng 2016;94 (12):2276–81.
[21] Ilka, Mahdi et al; Influence of Surface Defects and Size on Photochemical Properties of SnO_2 Nanoparticles, Materials (Basel, Switzerland) vol. 11,6 904. 28 May. 2018.
[22] Aydın C. Synthesis of SnO2:rGO nanocomposites by the microwave-assisted hydrothermal method and change of the morphology, structural, optical and electrical properties. J Alloy Compd 2019;771:964–72.
[23] Jana R, Sil S, Dey A, Datta J, Ray PP. Analysis of temperature dependent electrical performance of Al/CuO/ITO Schottky barrier diode and explanation of inhomogeneous barrier heights by double Gaussian distribution. AIP Adv 2018;8 (12):125104.
[24] Tomer D, Rajput S, Li L. Spatial inhomogeneity in Schottky barrier height at graphene/MoS2 Schottky junctions. J Phys D: Appl Phys 2017;50(16):165301.
[25] Sağlam M, Güzeldir B, Türüt A, et al. Role of Reduced Graphene Oxide-Gold Nanoparticle Composites on Au/Au-RGO/p-Si/Al Structure Depending on Sample Temperature. Journal of Elec Materi 2021;50:4752–61.
[26] Mikhelashvili V, Eisenstein G, Garber V, Fainleib S, Bahir G, Ritter D, et al. On the extraction of linear and nonlinear physical parameters in nonideal diodes. J Appl Phys 1999;85(9):6873–83.
[27] Baltakesmez A, Sevim M, Güzeldir B, Aykaç C, Biber M. Interface application of NiPt alloy nanoparticles decorated rGO nanocomposite to eliminate of contact problem between metal and inorganic/organic semiconductor. J Alloy Compd 2021;867:158802.
[28] Alialy S, Altındal Ş, Tanrıkulu EE, Yıldız DE. Analysis of temperature dependent current-conduction mechanisms in Au/TiO2/n-4H-SiC (metal/insulator/ semiconductor) type Schottky barrier diodes. J Appl Phys 2014;116(8):083709.
[29] ZeyrekI S, Bülbül MM, Altındal Ş, Baykul MC, Yüzer H. The double gaussian distribution of inhomogeneous barrier heights in Al/GaN/p-GaAs (MIS) schottky diodes in wide temperature range. Braz J Phys 2008;38(4).
[30] Turut A. On current-voltage and capacitance-voltage characteristics of metal-semiconductor contacts. Turkish J Phys 2020;44(4):1.
[31] Saghrouni H, Missaoui A, Hannachi R, Beji L. Investigation of the optical and electrical properties of p-type porous GaAs structure. Superlattices Microstruct 2013;64:507–17.
[32] Gümüş A, Türüt A, Yalçin N. Temperature dependent barrier characteristics of CrNiCo alloy Schottky contacts on n-type molecular-beam epitaxy GaAs. J Appl Phys 2002;91:245.
[33] Güçlü ÇŞ, Özdemir AF, Altindal Ş. Double exponential I-V characteristics and double Gaussian distribution of barrier heights in (Au/Ti)/Al2O3/n-GaAs (MIS)-type Schottky barrier diodes in wide temperature range. Appl Phys A 2016;122: 1032.
[34] Cetin H, Ayyildiz E. Temperature dependence of electrical parameters of the Au/n-InP Schottky barrier diodes. Semicond Sci Technol 2005;20:625.
[35] Iucolano F, Roccaforte F, Giannazzo F, Raineri V. Temperature behavior of inhomogeneous **Pt/GaNPt/GaN** Schottky contacts. Appl Phys Lett 2007;90: 092119.
[36] Das M, Datta J, Dey A, Halder S, Sil S, Ray PP. Temperature dependent properties of Al/rGO-ZnCdS Schottky diode and analysis of barrier inhomogeneities by double Gaussian distribution. Mater Lett 2017;204:184–7.
[37] Pakma O, Serin N, Serin T, Altındal Ş. The double Gaussian distribution of barrier heights in Al/TiO2/p-Si (metal-insulator-semiconductor) structures at low temperatures. J Appl Phys 2008;104:014501.
[38] Laurent MA, Gupta G, Suntrup DJ, DenBaars SP, Mishra UK. Barrier height inhomogeneity and its impact on (Al, In, Ga)N Schottky diodes. J Appl Phys 2016; 119:064501.
[39] Ouennoughi Z, Toumi S, Weiss R. Study of barrier inhomogeneities using I-V–T characteristics of Mo/4H–SiC Schottky diode. Physica B 2015;456:176–81.
[40] Aydoğan Ş, Sağlam M, Türüt A. On the barrier inhomogeneities of polyaniline/p-Si/Al structure at low temperature. Appl Surf Sci 2005;250(1–4):43–9.